Lightweight and high-security laser-based cotton tip pruning robot

Xuan'ang Guo, Ziyang Mao[1], Zedong Shi, Wei Lu*
(*School of Artificial Intelligence, Nanjing Agricultural University, Nanjing 210031, China*)

Abstract: Considering the current environmental pollution caused by chemical topping, plant damage caused by mechanical topping, and the high cost of manual topping, a laser-based cotton-tip pruning robot for field cotton was designed in this study. The main advantages of this robot include its safety, light weight, low cost, and environmental friendliness. First, the structural design, measurement, and corresponding control system design of the robot were realized. Subsequently, a precise laser control method based on Yolov5 cotton top identification and the inverse kinematic solution of parallel robot rapid positioning were examined. Subsequently, the optimal laser irradiation wavelength and duration were determined. Finally, a laser-topping experiment was conducted, and the overall accuracy and recall rates for cotton identification were 98.3% and 99.3%, respectively. The AP and mAP at the threshold value of 0.5 reached 99.3% and 78.8%, respectively. The maximum positioning error of the jacking system is 2.6 mm, and the repeated positioning error is within ±1.2 cm, which meets the accuracy requirements of laser jacking. Blue-purple laser irradiation at 15 W and 405 nm for 22 s was the best topping scheme. Comparing the effects of cotton topping with and without manual topping, it can be seen that laser topping significantly improved the yield and quality. Combined with the photothermal response of the cotton topping, the feasibility of laser topping was verified both theoretically and experimentally. The laser-topping scheme proposed in this study exhibits high efficiency, environmental protection, and safety, as well as good application prospects.

Keywords: laser topping, parallel manipulator, photothermal response, object detection
DOI: 10.25165/j.ijabe.20241704.8385

Citation: Guo X A, Mao Z Y, Shi Z D, Lu W. Lightweight and high-security laser-based cotton tip pruning robot. Int J Agric & Biol Eng, 2024; 17(4): 98–108.

1 Introduction

Cotton is an important strategic and industrial raw material with the widest industrial network in the planting industry and contributes to the development of the national economy[1]. Cotton topping[2] is a crucial step in the cotton growth process that affects the yield and quality of cotton. Cotton topping involves the removal of growth points on the main branches when the cotton grows to a predetermined height to restrain the wild growth of cotton, promote the development of side branches, ensure the availability of nutrients required for boll setting, and effectively promote high cotton yield. In addition to traditional manual topping[3], other topping methods can be divided into mechanical[4] and chemical topping[5]. Mechanical topping often involves the use of a hydraulic system, and the height of the crops is obtained via lasers, ultrasonics, gratings, and other sensors. The cotton top is then physically cut considering the empirical topping size data to perform cotton topping. Several types of mechanical topping equipment are available. For example, Gravalos et al.[6] developed a tobacco mechanical top-bud beating and armpit bud control high-gap mobile robot. Zhou et al.[7] designed a self-propelled cotton top machine. Compared with manual top-beating, this method has a higher efficiency and reduces labor intensity; however, it inevitably damages cotton buds and bolls, sacrificing the yield at the top of the crop. Chemical topping employs bud suppressors to inhibit cell division and elongation in the top part of the cotton to realize automatic cotton top capping. Chemical topping robots, such as the chemical control topping robot developed by Brar et al.[8] and other teams at the Punjab Agricultural University in India, have long been studied worldwide. Chemical topping is a simple, convenient, and effective method, and problems such as physical injury caused by artificial and mechanical topping, long time spans, missed topping, or repeated topping can be avoided to the maximum extent. However, improper use of chemical topping agents can cause drug damage to crops, hinder later growth, and lead to high economic risks. There are also potential hazards such as water and soil pollution[9].

Compared with traditional cutting tools and shoot suppressors, lasers[10] allow a high speed, noncontact, and eco-friendly operation, reducing the possibility of crop disease infection. With the rapid development of artificial intelligence, machine vision combined with lasers has been widely applied in agriculture[11]. Zhu et al.[12] designed a weeding robot based on the YOLOX convolutional neural network for weeding corn seedling fields. This robot calculates the coordinates of weeds using the triangle similarity principle and a single visual distance, and the end actuator of the robot arm, which can be controlled, emits a laser to kill weeds. The research and development team of Microsoft[13] developed a millisecond “laser gun” mosquito and fly killing system that identifies insects by the frequency of their wings beating and then locates target insects based on machine vision to select the optimal laser pest control scheme. Carbon Robotics, an American company, designed a tractor-sized self-guided laser-weeding robot. The robot uses high-speed cameras, deep learning, and other technologies to identify and locate weeds, then removes them using a high-power CO_2 laser. Compared to traditional spray weeding, this weeding method reduces the risk of soil and water pollution. A comparison of the three topping methods is listed in Table 1.

In this study, aimed at a complex field environment and standardized cotton planting and agriculture, a laser-topping mobile

Received date: 2023-06-10 **Accepted date:** 2024-05-07
Biographies: Xuan'ang Guo, BS, research interest: agricultural robotics, Email: xuangg@stu.njau.edu.cn; **Ziyang Mao**, BS, research interest: agricultural robotics, Email: njau_ziyangm@163.com; **Zedong Shi**, MS, research interest: agricultural machinery, Email: 2993463870@qq.com.
***Corresponding author: Wei Lu**, Professor, research interest: intelligent robotics and advanced non-destructive detection technology in agriculture. College of Artificial Intelligence, Nanjing Agricultural University, Nanjing 210031, China. Tel: +86-13951723465, Email: njaurobot@njau.edu.cn.

Table 1 Mode comparison

Topping mode	Features	Example
Manual topping	Time-consuming, laborious and inefficient	Traditional way[3]
Chemical topping	High efficiency, reduced labor, physical damage	Ioannis Gravalos[6]
Mechanical topping	Simple, convenient, quick effect, crop damage, pollution	Team of Harjeet Singh Brar[8], Punjab Agricultural University, India
Laser topping	High speed, no contact, environmental protection	The way this article is designed

robot with a high gap, light weight, low cost, and green cleaning was designed. The robot utilizes the Yolov5 algorithm to perform real-time detection of the cotton top and controls the delta parallel manipulator through kinematic analysis for further control of the laser to perform the topping task. The actual parameters of laser topping are determined according to the photothermal characteristics of the cotton-top structure, and the feasibility of this method is analyzed based on this principle.

2 Materials and methods

2.1 Technical route

This study designed the configuration according to cotton planting agronomy and growth characteristics of the cotton bud stage. The robot's measurement, control, and communication systems were designed according to the robot's man–machine interaction requirements. Through photothermal response and physiological analysis of the cotton top, the key parameters of laser topping were determined. The model training based on deep learning obtains the position information of the cotton top and realizes its target positioning of cotton top. Finally, a prototype was built, and a key performance test was conducted to meet the requirements of use. Figure 1 presents the corresponding technical roadmap.

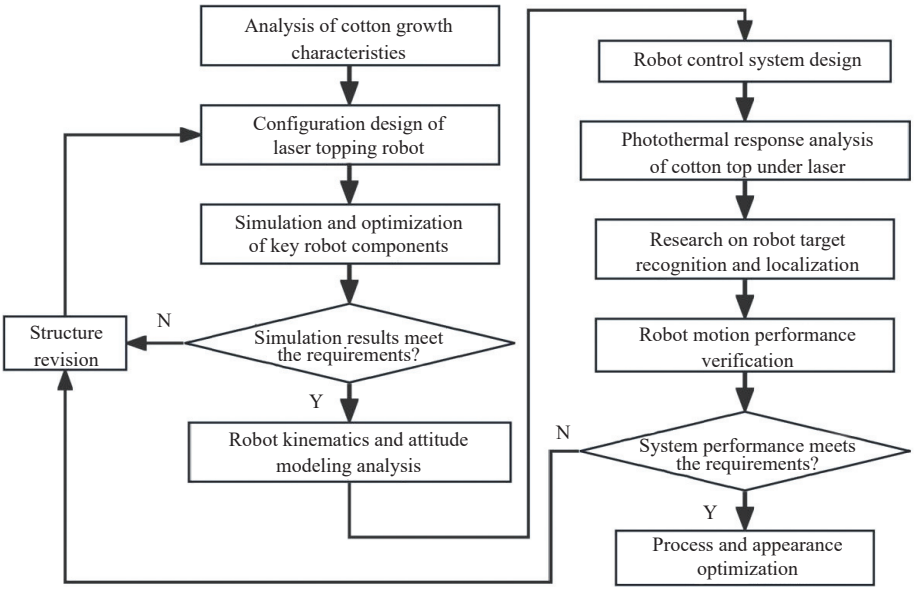

Figure 1 Development process of laser topping mobile robot

2.2 Complete machine structural design

The prototype laser-topping robot comprised three subsystems: the robot moving platform, movement and steering control, and the power supply system for the entire robot. Cotton identification and topping were performed using a machine-vision topping system. The control system was responsible for the overall control of the laser-topping robot. Based on the design of a standardized cotton-production environment, the row spacing for cotton planting in the field was 85-95 cm, the width of the ridge was approximately 40 cm, and the plant height at the cotton-bud stage was between 65-75 cm. The bottom height of the robot was 100 cm, the wheel spacing was 78 cm, and the wheel width was 36 cm. The motion height of the parallel robot ranged from 10 to 20 cm, as shown in Figure 2.

2.3 Robot mobile platform design

The mobile platform of the robot ensures that the entire topping robot system operates normally, and includes a four-wheel front-drive structure, steering mechanism, and power-supply system. The four-wheel front-drive structure includes an aluminum profile frame, device-fixed platform, universal wheel, C20-400LR hub motor, and front fork. The steering mechanism included an L-type Z2BLD stepper motor, direction machine, universal joint, fisheye bearing, and bowl set to control the steering of the robot. The power supply included four 12 V lithium batteries and monocrystalline silicon solar photovoltaic (PV) panels. Figure 3 illustrates the specific layout.

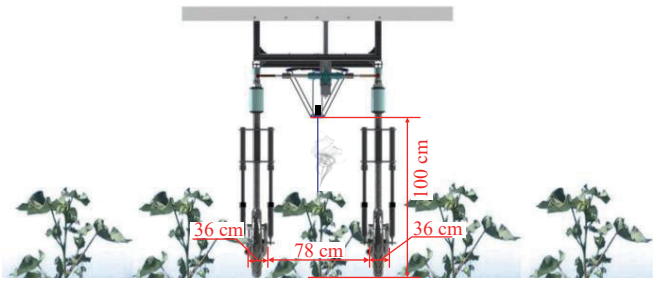

Figure 2 Running state of robot on cotton field

The DC motor of the steering device is connected to the drive shaft of the steering machine through a universal joint, and the ball head pins at both ends of the steering machine are fixed by fisheye bearings and the directional columns of the two front wheels. The welded concave connectors of the tie-rod support of the steering machine are fixed to the body using a bolted connection. Therefore, when the motor deflects, the bottom gear teeth close the rack, and the steering machine has a relative displacement, driving the tie rod to rotate the wheel in the same direction as the deflection to achieve wheel deflection, resulting in an Ackermann Angle.

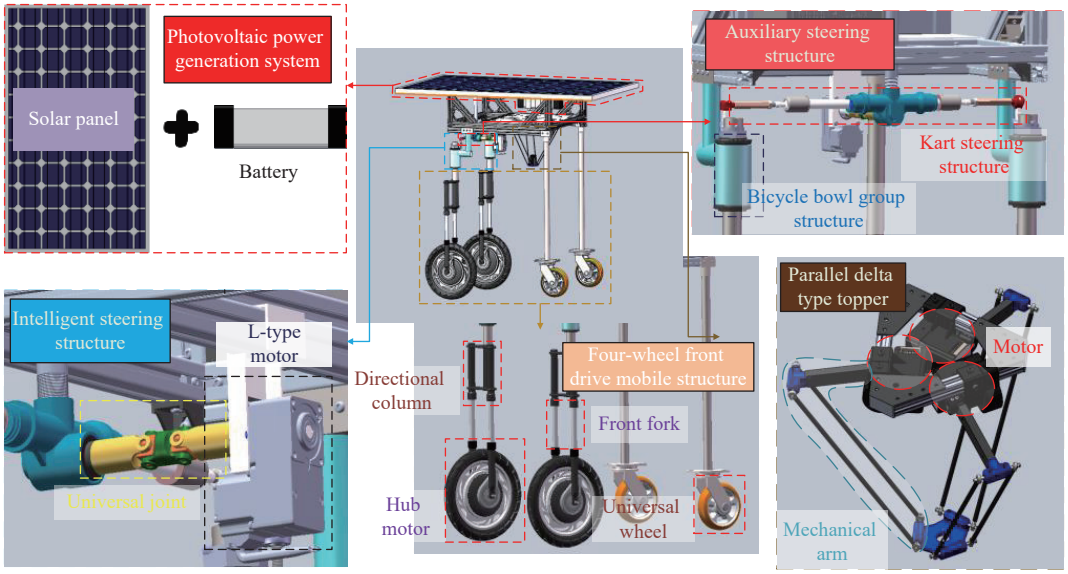

Figure 3 Robot mobile platform structure

2.4 Motion control method of parallel robot based on vision

An RGB-D camera (D435i) was selected for image acquisition, obtained the internal and external parameters of the camera using the checkerboard calibration method, calibrated the camera, and trained the cotton-top recognition model using the Yolov5 algorithm, which returned the top coordinates of the cotton-top region. The width and height data of the cotton-top region, combined with internal camera parameters and depth data, were converted into a world coordinate system. The angle of the robot is determined using the inverse kinematic solution of the parallel manipulator. After reaching this position, the laser switching quantity was controlled to achieve the topping. This process is illustrated in Figure 4.

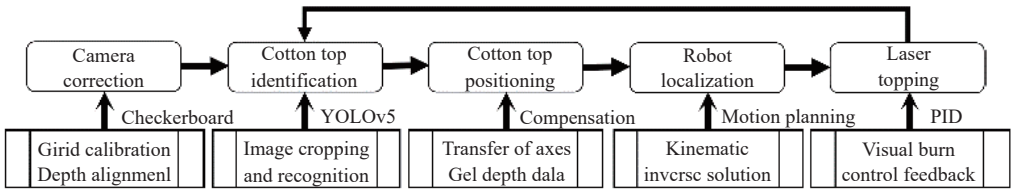

Figure 4 Block diagram of kinematic control method for parallel robot based on vision

2.4.1 Camera calibration

This system uses the camera calibrator function package in the MATLAB R2022a software to calibrate the camera. A checkerboard template of 8 rows and 11 columns with width of 15 mm was used. After printing this onto A4 paper, the shooting angle was adjusted and 37 checkerboard grids were captured. The automatic focus test showed that the corner pixel error of each image was less than 0.25, which conformed to the maximum error threshold of 0.5, for camera calibration.

The internal parameter matrix of the camera is:

$$K = \begin{bmatrix} 901.23 & -0.43 & 671.25 \\ 0 & 900.97 & 352.77 \\ 0 & 0 & 1 \end{bmatrix}$$

An infrared sensor camera can obtain depth information by analyzing speckle images using the depth level and parallax map combined with the reference image. The mapping relationship between the depth camera and the color camera is as follows:

$$Z_{rgb} p_{rgb} = K_{rgb} P'_{rgb} \tag{1}$$

where, Z_{rgb} is the scale factor of the color camera, $p_{rgb} = [u, v, 1]^{\mathrm{T}}$ is the coordinate expression projected onto the pixel coordinates, K_{rgb} is the internal reference of the color camera.

Similarly, the mapping relation of the depth camera can be obtained as follows:

$$Z_{ir} p_{ir} = K_{ir} P'_{ir} \tag{2}$$

Assuming that the external parameters of the color camera are R_{rgb} and T_{rgb}, and the external parameters of the depth camera are R_{ir} and T_{ir}, for the nonchiral coordinate representation of the respective camera coordinate system under the three-dimensional points P'_{ryd} and P'_{ir} the following relationship exists:

$$P'_{rgb} = R_{rgb} R_{ir}^{-1} P'_{ir} + T_{rgb} - R_{rgb} R_{ir}^{-1} T_{ir} \tag{3}$$

A depth image was adopted to align the RGB image owing to the high real-time requirements of the cotton-top operation. The results of the alignment tests are presented in Figure 5.

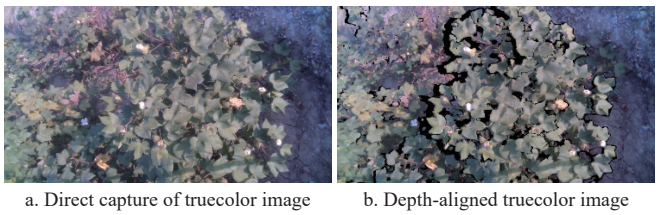

a. Direct capture of truecolor image b. Depth-aligned truecolor image

Figure 5 Depth alignment before and after test

2.4.2 Cotton top identification

A cotton-top recognition algorithm model based on the YOLOv5-TL deep neural network is selected for this system[14,15]. Real-time images were obtained using a depth camera and convolved with each input image using a two-dimensional Gaussian smoothing filter having a size of 3×3 and σ=3 to obtain the output image[16]. The cotton-top RGB and gray color thresholds were set,

and the obtained images were subjected to corrosion and expansion processing to complete the open operation. The gradient image was then subjected to threshold processing to reduce image over-segmentation. After binarization, the gray image was judged based on the pixel area[17], and the recognition area with a small area was identified as interference and discarded. The identified cotton-top block was then determined to be elliptical, and the cotton-top image was further framed[18].

The cotton-top image dataset comprised Dayu Mianbao 21 cotton grown in a greenhouse POTS. From July 10 to July 15, depth cameras were used to collect the top data at multiple scales at 8:00, 15:00, and 18:00 every day. A total of 1650 effective images were collected, two of which are displayed in Figure 6.

Figure 6 Source of cotton-top image dataset

The acquired images were manually labeled using the Labellmg image labeling software and divided into five categories: top, leaf, bolt, bud, and flower. The label is based on the minimum value outside the target. Owing to the small amount of cotton-top data, 7980 pieces of data were expanded through horizontal and vertical image flipping and brightness adjustment[19] to avoid deep-learning network overfitting. The dataset was divided into training, verification, and test sets in a ratio of 6:2:2. The structure adopts the COCO128 format.

2.4.3 Cotton top positioning

The model returns the top coordinates as well as the width and height data of the cotton-top region $[x_0, y_0, w, h]$, where $[x_0, y_0]$ are the anchor-point coordinates of the cotton-top region and the pixel coordinates of the cotton-top center are $\left[x_0+\frac{w}{2}, y_0+\frac{w}{2}\right]$, to obtain the depth information of the cotton-top detected and selected in the alignment depth map[20]. Second, the internal parameters of the camera were calculated, including the focal length (f_x, f_y) and main points (c_x, c_y).

$$\begin{cases} z = depth \\ x = \dfrac{\left(x_0+\dfrac{w}{2}-c_x\right)\cdot z}{f_x} \\ y = \dfrac{\left(y_0+\dfrac{w}{2}-c_y\right)\cdot z}{f_y} \end{cases} \tag{4}$$

The corresponding coordinates of all pixels in the selected cotton-top detection rectangle were obtained according to Equation (4). The average value was used to calculate the camera coordinates at the top of the cotton sheet. The external parameters of the camera were then determined according to the positional relationship between the camera and the robot arm, and the world coordinates of the cotton top were obtained[21,22].

2.4.4 Robot localization

Considering the center point of the static platform of the parallel manipulator as the origin of the world coordinate system, a Cartesian coordinate system was established. The parallel manipulator comprises a static platform $\Delta Q_1Q_2Q_3$, moving platform $\Delta M_1M_2M_3$, three driving arms Q_iN_i, and three driven arms N_iM_i, $i=1,2,3$, where, O is the center point of the static platform, P is the center point of the moving platform, R is the external radius of the static platform, and r is the external radius of the moving platform, as depicted in Figure 7.

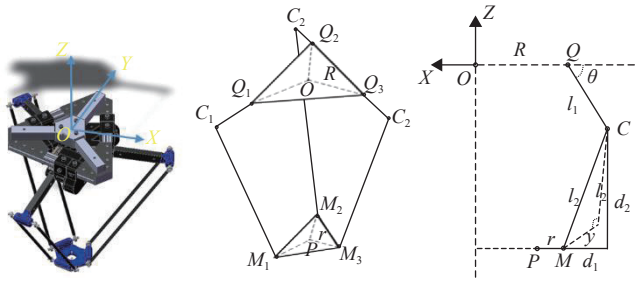

Figure 7 Space coordinate map of parallel manipulator

The center point $P(x,y,z)$ of the moving platform was determined to be 0.7 cm above the cotton top, and the *XOZ* section of the spatial coordinate system was selected to analyze a single connecting rod. R is the distance between the top of the driving arm and the center point, r is the distance between the end of the driven arm and the center point of the moving platform, θ is the angle between the driving arm and the *X*-axis, l_1 is the length of the driving arm, l_2 is the length of the driven arm, l_2' is the projection of the driven arm on the cross section of the driving arm, orthogonal to the *Y*-axis, d_1 is the projection of l_2 in the *Z*-direction of the *XOZ* plane, d_2 is the projection of l_2 in the *X*-direction of the *XOZ* plane.

The following relation can be obtained from the section coordinate system:

$$d_1^2 + d_2^2 = l_2^2 \tag{5}$$

$$l_2'^2 + y^2 = l_2^2 \tag{6}$$

$$R + l_1\cos\theta = -x + r + d_1 \tag{7}$$

$$d_2 = z + l_1\sin\theta \tag{8}$$

Let $T = R + x - r$ in Equations (5)-(8), and the following can be obtained:

$$l_1^2 - l_2^2 - x^2 - z^2 - T^2 = 2Tl_1\cos\theta + 2zl_1\sin\theta \tag{9}$$

For $G = l_1^2 - l_2^2 - x^2 - z^2 - T^2$, by incorporating the geometric relationship of Equation (10) into Equation (9), then Equation (11) is obtained.

$$\begin{cases} \cos\theta = \dfrac{1-t^2}{1+t^2} \\ \sin\theta = \dfrac{2t}{1+t^2} \\ t = \tan\left(\dfrac{\theta}{2}\right) \end{cases} \tag{10}$$

$$e_1t^2 + e_2t + e_3 = 0 \tag{11}$$

where, $e_1 = 2Tl_1 + G, e_2 = -4zl_1$, and $e_3 = -2Tl_1 + G$. Using the quadratic solution equation of one variable to calculate t and substituting it into Equation (11), θ can be obtained as follows:

$$\theta = 2\arctan\left(\frac{\pm\sqrt{e_2^2 - 4e_1e_3} - e_2}{2e_1}\right) \tag{12}$$

Therefore, joint angle $\theta = f(x,y,z)$ of the first active arm can be calculated, and the angle of other active arms can be determined similarly[23]. Because a delta robot is limited by its motion angle in the operating space, not all solutions satisfy these requirements. The inverse solution of the kinematics of the delta high-speed parallel

robot can be obtained by judging the value of "±" combined with the actual situation[24]. The angle of the robot was determined after it reached this position, and the laser switching quantity was controlled to achieve topping.

2.5 Control system design

The core of the robot was a measurement and control system. Through the measurement and control system, the robot could drive the motor, detect the target and cotton top, as well as control the quantity of laser switching and remote communication. The measurement and control system adopts a modular design, and the hardware part of the measurement and control system is mainly divided into the main control, mobile, steering, parallel manipulator, laser, and sensing modules. The main control layer was composed of an industrial computer, artificial intelligence processing hardware, and a control board. The industrial computer, as the main control terminal, is the core of the entire measurement and control system, which mainly includes the control of walking and steering through the RS485 electrical interface, processing and analysis of the sensor and position information sent by the lower computer, sending corresponding instructions to each module of the lower computer, and a remote real-time interaction function. Artificial intelligence processing hardware collects RGB image data, depth information, acceleration, and angular velocity data through a depth camera, combines powerful computing power, obtains the position data and confidence of the cotton top from the depth model in real time, and provides feedback to the industrial computer in real time. The control board was developed using an Arduino control board. It controls three drive modules through the Ramps1.4 integrated circuit to realize coordinated control of the parallel manipulator. When the main control end sends the position information of the cotton top, the control board controls the parallel manipulator to reach the specified position, and laser topping is completed by the pulse control of the switching amount of the laser. The moving and steering control modules are directly connected to an industrial computer through the RS485 bus to control the walking and steering of the robot and obtain its relative position information. Sensors mainly include an Intel depth camera and an industrial camera for real-time acquisition of cotton image information, depth information, and robot inertial data. The main purpose of an industrial camera is to obtain road condition information and feed it back to a remote client in real time, thereby providing a decision-making basis for the staff and ensuring the safety of the entire robot movement. The laser module controls the laser frequency, pulse width, and working time using the pulse signal sent by the lower machine. This is the end effector of the laser-topped mobile robot. The robot and remote worker communicate through the remote LAN built by the wireless bridge, and the overall scheme of the measurement and control system is shown in Figure 8.

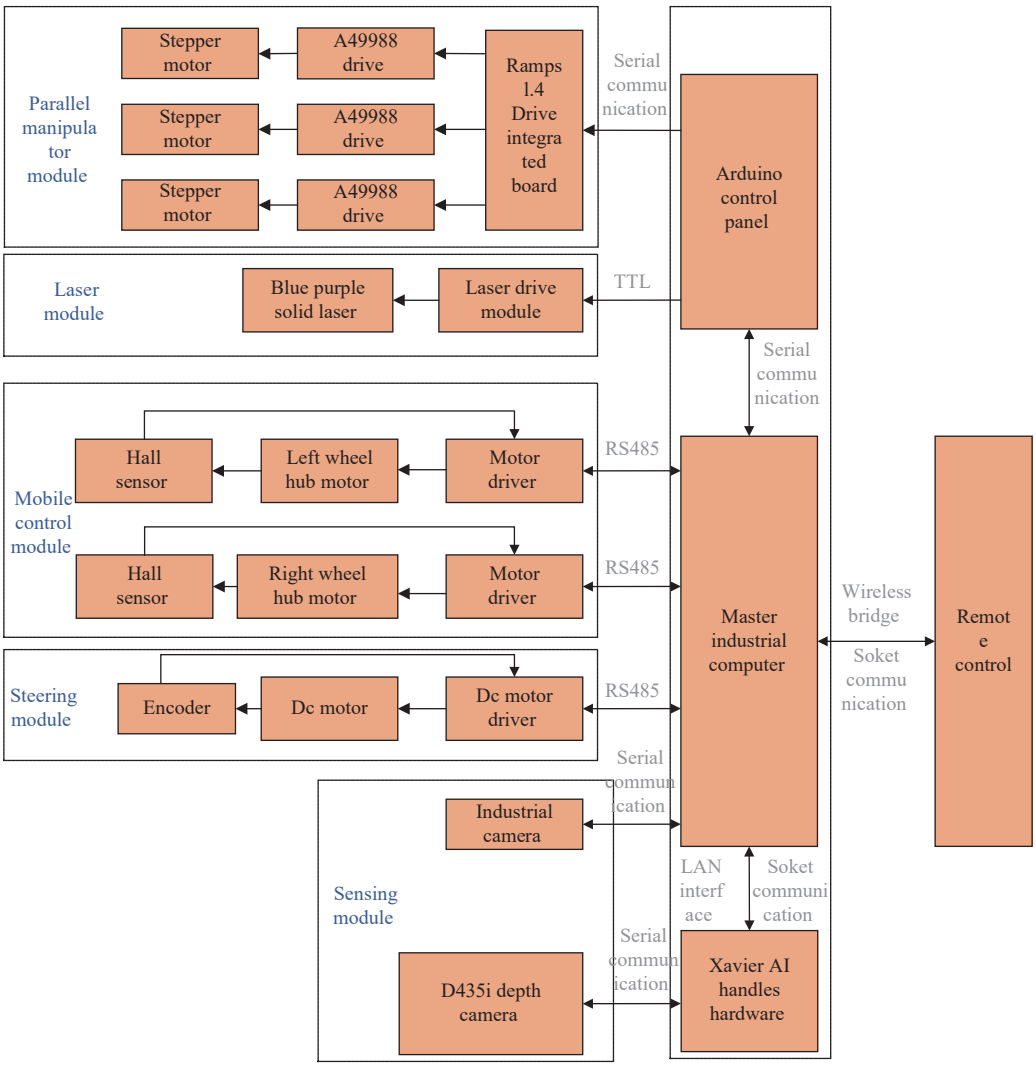

Figure 8 Overall design of the measurement and control system

The working flow of the topping robot is shown in Figure 9. The system initializes the client, contacts the server, and sends instructions to the robot to move along a straight line in a cotton field. During this period, the speed of the walking system was

controlled. When the position of the cotton top was detected, the walking control system was converted into position control. The angle of the robot was determined, the loaded laser was positioned according to the cotton top, and the laser topping was controlled through a pulse signal to control the laser frequency, pulse width, and working time. After the topping is completed, the manipulator is reset, and the status is set to idle. The robot continued to move and automatically turned according to the position control after finishing a row of cotton top buds until the entire topping task was complete.

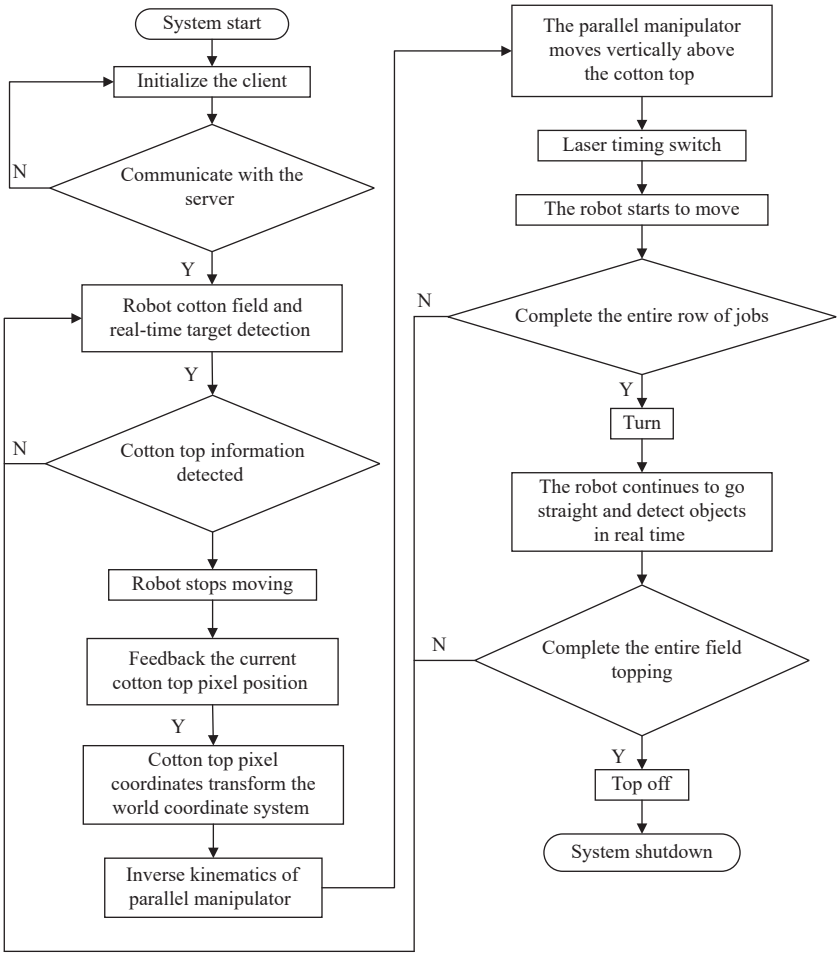

Figure 9 Flowchart of laser topping mission control

3 Results and discussion

3.1 Determination of photothermal response of cotton top tissue

3.1.1 Cotton top structure

The center of each leaf contained a cotton core. The horizontal diameter and depth of the cotton core were approximately 34 and 18 mm, respectively. The cotton-top tissue can be regarded as a cylindrical pipe. Figure 10 shows the top organizational structure of the cotton industry. A high-power laser that passes through when focused on a single point may cause unnecessary damage to cotton organs. Therefore, the system chooses a relatively low energy density topping mode, regarding the physical size of the plant tissue, by measuring the relationship between the laser distance and laser radius, which approximately determines the distance between the laser and the target object as 7-20 cm, at which point the spot diameter is approximately 0.8-5.0 cm.

Figure 10 Cotton top structure size

3.1.2 Determination of basic optical properties of cotton tops

In this study, a single integral system[25] was adopted as the measurement system to obtain the optical properties of cotton-top tissues. A single integrating system includes a halogen tungsten lamp, optical fiber, single integrating sphere, spectrometer, collimator, and other devices. Transmission and reflection experiments were conducted on five groups of cotton tops. The data results were averaged and anomalies were removed, as shown in Figure 11.

The reflection and transmission of the cotton-top tissue were the lowest at 400-500 nm. Therefore, a fixed blue–purple laser with the wavelength of 405 nm in blue-purple[26] was selected as the laser source for laser topping.

3.1.3 Histomorphology and physiological changes of cotton top under varying laser duration

Based on the photothermal response, a better effect was achieved when the laser measuring distance from the cotton top was

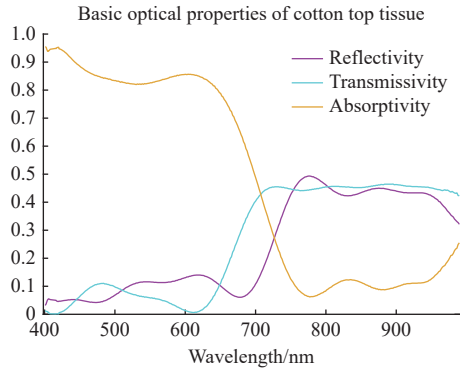

Figure 11 Reflection, transmission, and absorption spectra of cotton top tissue

7 cm, and the laser spot diameter was 0.8 cm. The cotton was divided into three groups according to the duration of laser irradiation (10 s, 22 s, or 36 s). The same water and fertilizer management practices were adopted in this study. Morphological changes in the cotton tops were observed every five days, as shown in Figure 12, and relevant physiological data were recorded.

As shown in Table 2, the absolute growth rate of cotton was the highest after 10 s of irradiation, whereas it was the lowest after 36 s of irradiation. Combined with the data on changes in plant branch and leaf lengths, the growth rate was fastest at 22 s, and the topping effect was the best. Therefore, the laser spot diameter of 0.8 cm was selected for the design of this system. Additionally, the irradiation duration of 22 s was considered for the laser topping scheme.

3.2 Cotton top recognition model training results

The proposed system adopted the Yolov5s model with depth_multiple = 0.33 and width_multiple = 0.50. The effect of the functional transformation trend in the Yolov5s model training is shown in Figure 13.

box_loss represents the loss function value of the prediction frame, i.e., the loss function of the IoU, obj_loss represents the target loss function, and cls_loss represents the loss function of confidence. When the epoch reached approximately 25, the loss function declined gradually and the model stabilized. The effects of the training are presented in Figure 14.

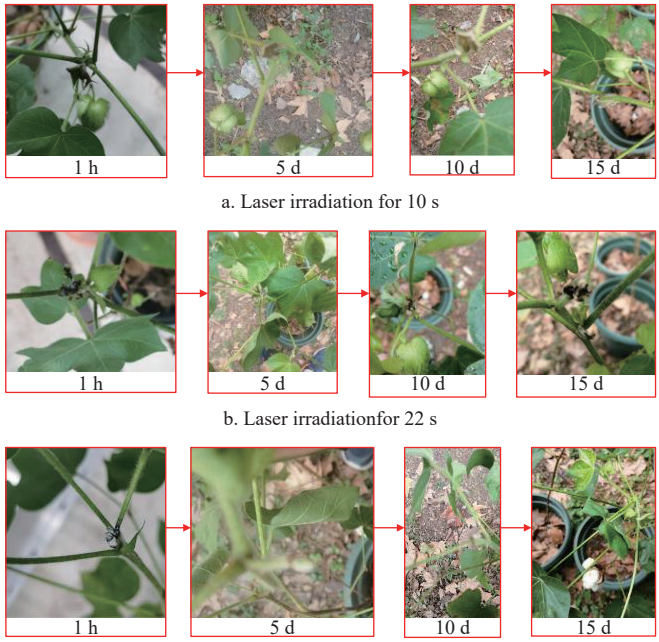

Figure 12 Changes in long duration cotton top under different irradiation times

Table 2 Growth data of cotton top after irradiation

Irradiation duration/s	Relative growth height of main stem/cm			Mean leaf length/cm			Mean branch length/cm		
Time	6.25	6.30	7.5	6.25	6.30	7.5	6.25	6.30	7.5
10	0.40	1.4	2.3	13.47	13.52	13.65	8.26	8.46	9.06
22	–1.5	0.3	0.5	13.56	14.58	14.66	8.76	9.26	9.55
36	–2.4	0.3	0.4	13.45	13.25	13.56	8.13	8.15	8.55

From the test results, the overall accuracy rate of cotton recognition was 98.3%, the recall rate was 99.3%, the threshold value of 0.5 AP was up to 99.3%, the mAP was as high as 78.8%, and the accuracy index met the requirement of topping. The detection time for the image sequences tested on the artificial intelligence hardware platform was 0.011 s per frame. The real-time cotton-top detection standards are listed in Table 3.

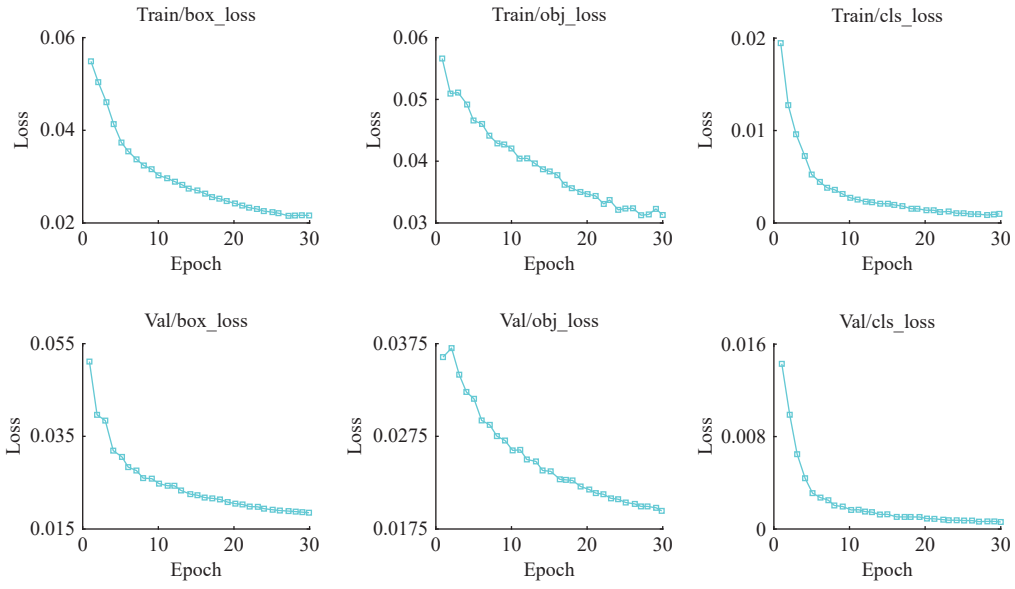

Figure 13 Training loss curves of the model

3.3 Topping system positioning test

The depth data and corner points of the images were obtained using a checkerboard. After determining the inverse and positive kinematic solutions of the parallel manipulator, the laser point

coordinates were marked on checkerboard paper to record the error data on the *X*- and *Y*-axes. A laser rangefinder was used to measure the *Z*-axis of the data. The distance between the center of the moving platform and the target height was set to the fixed value of 30 cm, and the grid size of the checkerboard paper was 1 cm. In the experiment, five coordinate points were randomly selected for recording, and the experiment was repeated thrice to record the repeatability error. The results are shown in Figure 15.

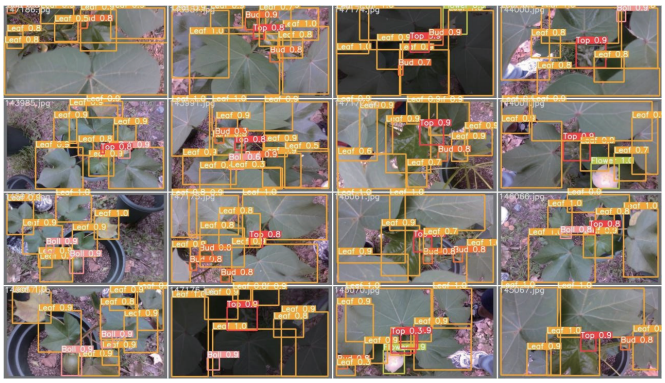

Figure 14 Test set effects

Table 3 Training result parameters

Class	Precision	Recall	AP@.5	mAP@.5:0.95
Top	98.9%	98.7	0.993	0.719
Boll	98.4%	1	0.994	0.776
Bud	98.2%	98.9	0.993	0.689
Leaf	97.2%	99.1	0.995	0.869
Flower	98.6%	1	0.992	0.888

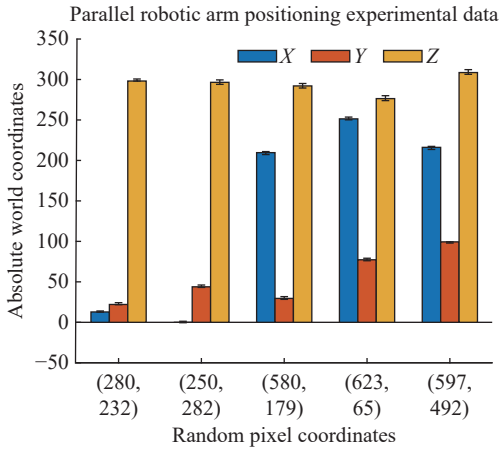

Figure 15 Results of topping system positioning test

It can be seen from the data that compared with the simulation results, the maximum error of horizontal plane and repeated positioning error of parallel manipulator obtained from the experiment are ±2.6 mm and ±1.2 mm, respectively. There was a height deviation of approximately 2 mm. This is due to the depth and systematic errors of the depth camera. Analysis of the test results demonstrated the applicability of the robot in topping operations.

3.4 Experimental research on laser topping robot

3.4.1 Laser topping robot, measurement, and control system

Configuration and processing were completed according to the aforementioned design. A Yanling industrial computer was selected, and the central processor of the chosen CPU was a 7th-generation I5. Two optional RS232 ports and four serial USB ports were available. The industrial computer was responsible for the real-time data processing and control of each module. The AI hardware system uses a high-performance computing module, NVIDIA Jetson AGX Xavier development kit, with 6-core CPU, 384 CUDA cores, 48 tensor cores, 16G memory, 512G storage, which meet the requirements of real-time target recognition and location. A semiconductor laser with power of 15 W was employed. The Intel® RealSense® Camera D435i is an RGB-D camera that combines a true-color camera and a depth camera. An outdoor kilometer-level wireless bridge was incorporated for a remote LAN equipped with a logarithmic omnidirectional antenna to strengthen the wireless signal reception ability. The control and sensing equipment conformed to the preselected parameters, the circuit wiring and layout were established, and finally, the construction of the prototype for the topping robot was completed, as shown in Figure 16.

Figure 16 Physical prototype

3.4.2 Experiment and analysis of robot laser topping

In this experiment, the topper effect of the potted cotton was analyzed from July 14 to 16, 2022. The cotton species used was Dayu Mian Bao 21, which is suitable for growth in the Yangtze River Basin, as shown in Figure 17.

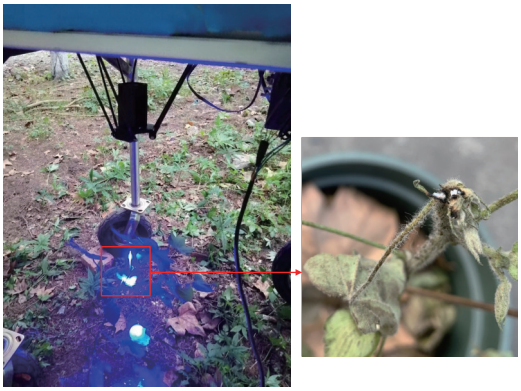

Figure 17 Robot cotton topping

The total number of experimental samples was 30, divided into three groups of 10: one group of samples was not topped, the second group was manually topped, and the third was laser topped under the laser spot diameter of 0.8 cm and topping time of 22 s. During the experiment, water and fertilizer management practices were unified. Plant trait data were recorded every 10 d until August 15. The data records are listed in Table 4.

The experimental data show that the height of the main cotton stem decreased significantly after 10 cm of core picking and that the growth trend was dominant and gentle. After laser topping, the plant showed soft tissue damage, which gradually atrophied and fell off spontaneously at approximately 15-20 s, whereas the cotton growth rate was dominant and gentle. Furthermore, the relative growth

number of cotton peaches increased significantly compared to that with other topping methods, and the average fruit branch length increased significantly, similar to that with artificial topping. The characteristics of cotton after different topping methods are presented in Figure 18.

Table 4 Cotton characteristics under different topping methods

Treatment mode	Mean relative growth height			Average number of peaches per plant			Mean fruit branch length		
Date	7.26	8.05	8.15	7.26	8.05	8.15	7.26	8.05	8.15
Untopped	10.12	8.52	5.76	4.2	4.5	4.7	7.06	8.82	10.38
Manual topping	–5.12	3.15	1.91	4.3	4.9	5.2	10.33	12.15	13.60
Laser topping	–2.50	–0.25	1.03	4.2	4.8	5.1	8.62	11.39	12.62

Figure 18 Growth state of cotton after adopting different topping methods

3.5 Discussion

3.5.1 Theoretical analysis of optical transmission

The traditional topping method uses one leaf and core. In addition to the top bud, the leaf closest to the meristem was included. The activity of the cotton bud was far lower than that of the cotton leaf; therefore, the top tissue of the cotton was similar in structure to that of the cotton leaf. The transmission process of light[27] in the blade was simulated using the blade model: when the light is incident on the surface of the plant tissue, a small part of the incident light forms a diffuse reflection in the upper epidermis of the plant, and the rest of the light enters the interior of the tissue. Part of the scattered light is reflected in the palisade layer, and the rest of the scattered light passes through the lower epidermis to form transmitted light, part of which is absorbed by the chlorophyll and other pigments in the palisade tissue to convert photochemical energy and heat energy. Moreover, part of the light is absorbed, reflected, and transmitted by water in the spongy tissue, as depicted in Figure 19.

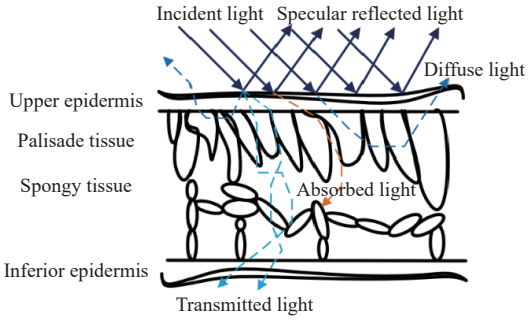

Figure 19 Leaf radiation transfer model client interface

From a macroscopic perspective, the light transmission in biological tissues can be used to approximate multiple scattering processes in random media. To solve this problem, the wave effect of light is ignored[28]. A definite model based on transmission theory was chosen accordingly, and the Beer-Lambert law[29] was adopted. This brief analysis provides a theoretical basis for determining the basic characteristic parameters of cottontop optics. The basic characteristics of plant light transmission were verified using a single integrating sphere system, and a 405 nm blue-purple laser was applied when the absorption rate was the highest.

3.5.2 Theoretical analysis of photothermal response of cotton top

The interactions between light and biological tissues include photothermal, photochemical, photopressor, and electromagnetic fields. In this study, the effect of light on the cotton top was primarily evaluated based on the thermal effects of light radiation[30,31]. Shi et al.[32] studied the responses of plants to light stress. The effects of laser irradiation on plants can be divided into five stages according to the time, as presented in Figure 20.

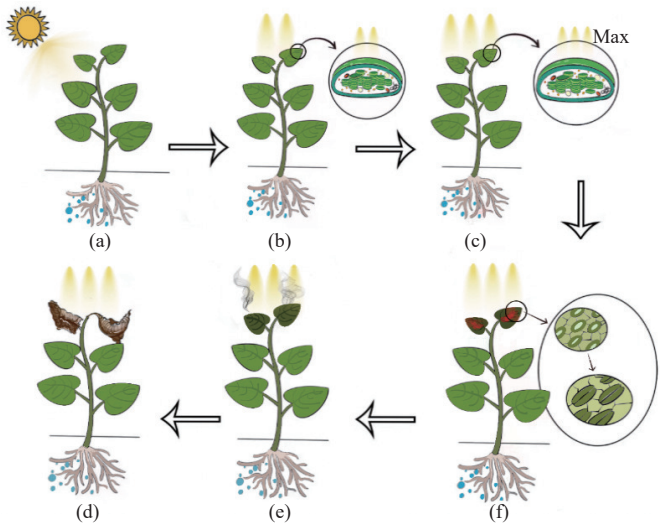

Figure 20 Effect of laser irradiation on plants

Figure 20a shows the initial normal solar irradiation followed by vertical laser irradiation.

Figure 20b shows the first stage of laser irradiation; the external light intensity changes in a very short time, but the light intensity experienced by the photosynthetic apparatus inside the plant gradually increases, and light is the main factor affecting photosynthesis[33]. Photosynthetic rate gradually increased with increasing light intensity.

Figure 20c shows the second stage of laser irradiation: when the light absorbed by plants reaches a certain intensity, the photosynthetic rate reaches a maximum, the light intensity continues to increase, and the photosynthetic rate remains unchanged, that is, the phenomenon of light saturation[34].

Figure 20d shows the third stage of laser irradiation. As the light intensity continues to increase, the utilization rate of light energy decreases, and the amount of light energy absorbed by the photosynthetic apparatus exceeds the amount that can be utilized by photosynthesis. Excess light energy leads to a decrease in photosynthetic rate and function, specifically photoinhibition[35,36]. Meanwhile, when the surface biofilm is destroyed, many metabolic processes cannot be carried out and permeability increases. At this time, the photosynthetic function of plants can be gradually restored after light is weakened, and considerable pigment loss generally does not occur, which is reversible.

Figure 20e shows the fourth stage of laser irradiation: the photosynthetic apparatus is exposed to strong light for a long time,

which causes irreversible damage to the plants. Photooxidation occurs because of the degradation of photosynthetic pigments and the destruction of photosynthetic mechanisms[37,38]. More importantly, when the temperature rises above a certain threshold, the water on the surface of biological tissues boils and generates a large amount of water vapor, which breaks through the cells and tissues and runs out, removing some cell fragments.

Figure 20f shows the fifth stage of laser irradiation. With a gradual increase in the temperature, the temperature of the dry tissue remaining after dehydration continued to increase. When the carbonization temperature was reached, a carbonization reaction occurred in the dry tissue and carbon black was precipitated, resulting in a carbonization effect[39].

According to the above experimental analysis, this is essentially the same as theory. This principle proves that the laser topping method is feasible and that the realization of topping does not require reaching the carbonization stage, which can inhibit the growth of the top bud, promote the growth of the side bud, complete the topping task, or save resources to reduce unnecessary casualties in other plant tissues. In the actual topping process, the duration of laser irradiation of 15 W with spot diameter of 0.8 cm can be 22 s.

3.5.3 Robot design scheme analysis

Focusing on the cotton field environment, the environmental constraints of the topping robot in the cotton-bud stage were analyzed, and a high-gap mobile platform for a typical robot was designed. The entire body of the robot comprises hollow aluminum profiles that reduce its weight while facilitating disassembly and assembly. An L-shaped structure was adopted to realize a stable connection between the front wheel and body, and the overall strength of the platform was enhanced via welding between the wheels. Enhanced stability and a symmetrical overall structure improve the motion of the robot over complex terrain. The maximum conversion efficiency of the PV power generation panel was 24%. The PV panel is directly connected to an industrial computer with four 12 V lithium batteries and is connected to other parts through a step-down module, which can save energy and meet the requirements of the system. The mobile system realizes a closed-loop speed control using a PID algorithm. The overshoot was small, and speed regulation was smooth at high speeds. The speed–position closed-loop control mode was adopted to control the steering motor angle. The wheel angle was determined according to the corresponding relationship between the measured data and the turning radius. The measurement and control system adopts a modular design to enhance the cohesion between the modules and reduce the degree of coupling, which is convenient for troubleshooting and reduces the risk of system failure. The industrial camera provides road information to ensure the safety of robot movement, whereas the laser uses vertical irradiation. This significantly improves the safety of the entire system, in addition to avoiding accidents caused by laser operation. Considering that all functions are integrated in the human–computer interaction software, the control or monitoring of the entire system is completed by the industrial computer, and interpersonal interaction, the entire system is more user-friendly and concise.

Moreover, the proposed system completes the motion control of a parallel manipulator based on vision. To ensure real-time detection, Yolov5 was selected as the model algorithm. With the enhanced cotton-top dataset, a model with an accuracy of up to 98.9%, recall rate of up to 99.3%, and mAP of up to 71.9% was trained, which could better realize cotton-top recognition. The pixel coordinates returned by the model are converted into world coordinates and combined with the inverse kinematics solution of the delta-parallel manipulator to realize an accurate topping task. The maximum positioning error was 2.6 mm and the repeated positioning error was ±1.2 cm, meeting the requirements of topping accuracy. Through a robot topping experimental analysis, laser topping significantly improved the production yield and quality compared with no topping, which verifies the rationality of the robot design scheme.

4 Conclusions

Aiming at a complex field environment and standardized cotton planting and agriculture, a laser-topping mobile robot with a large gap, light weight, low cost, and green cleaning was designed in this study. In addition, a laser-topping scheme based on machine vision was proposed, incorporating the Yolov5 algorithm to build a cotton-top recognition model with an accuracy of 98.9% and an mAP of 71.9%. Through visual coordinate transformation combined with delta-key technology, the accurate positioning of the cotton top was achieved with deviation of approximately 2 mm. The operating parameters of the system were analyzed and optimized through a cotton topping experiment. As a result, the best topping scheme was determined to be 15 W and 405 nm blue-purple laser irradiation for 22 s. In addition, the topping performance was tested. The overall feasibility of the system was verified from both theoretical and practical perspectives, and an efficient and contact-free scheme was developed for cotton-topping agriculture. Further optimization may involve appropriately increasing the laser power to improve the operational efficiency.

Acknowledgements

This work was supported in part by the Modern Agriculture Project of Jiangsu Province Science and Technology Plan Special Fund Project (Grant No. BE2022363), the Fundamental Research Funds for the Central Univerisities (Grant No. KYCXJC2024003) and the Modern Agricultural Machinery Equipment and Technology Demonstration and Promotion Project of Jiangsu Province (Grant No. NJ2022-03).

[References]

[1] Tokel D, Genc B N, Ozyigit I I. Economic impacts of Bt (*Bacillus thuringiensis*) cotton. Journal of Natural Fibers, 2022; 19(12): 4622–4639.

[2] Dai J, Tian L, Zhang Y, Zhang D, Xu S, Cui Z, et al. Plant topping effects on growth, yield, and earliness of field-grown cotton as mediated by plant density and ecological conditions. Field Crops Research, 2022; 275: 108337.

[3] Renou A, Téréta I, Togola M. Manual topping decreases bollworm infestations in cotton cultivation in Mali. Crop Protection, 2011; 30(10): 1370–1375.

[4] Sharma K, Chandel R. Multiple attributed parametric review on mechanical picking of cotton (*Gossypium Hirsutum* L.) crop in relevance to developing countries. Agricultural Mechanization in Asia, Africa and Latin America, 2021; 52(2): 7–13.

[5] Qi H, Xiao C, Zhao W, Xu D, Eneji A E, Lu Z, et al. Chemical topping with mepiquat chloride at flowering does not compromise the maturity or yield of cotton. Agronomy, 2023; 13(2): 497.

[6] Gravalos I, Ziakas N, Loutridis S, Gialamas T. A mechatronic system for automated topping and suckering of tobacco plants. Computers and Electronics in Agriculture, 2019; 166: 104986.

[7] Zhou H, Yin S, Zhu L, Yang X, Yan H. Design of 3WDZ-6 self-propelled cotton top cutting. Transactions of the CSAM, 2010; 41(S1): 86–89. (in Chinese)

[8] Brar H S, Kumar D, Singh P. Dataset of source-sink manipulation through growth retardant for enhancing productivity and profitability of cotton in north west, India. Data in Brief, 2020; 31: 105914.

[9] Nie J, Li Z, Zhang Y, Zhang D, Xu S, He N, et al. Plant pruning affects photosynthesis and photoassimilate partitioning in relation to the yield formation of field-grown cotton. Industrial Crops and Products, 2021; 173.
[10] Bai Z, Zhao Z, Tian M, Jin D, Pang Y, Li S, et al. A comprehensive review on the development and applications of narrow-linewidth lasers. Microwave and Optical Technology Letters, 2022; 64(12): 2244–2255.
[11] Abbas I, Liu J, Faheem M, Noor R S, Shaikh S A, Solangi K A, et al. Different sensor based intelligent spraying systems in Agriculture. Sensors and Actuators A: Physical, 2020; 316: 112265.
[12] Zhu H, Zhang Y, Mu D, Bai L, Zhuang H, Li H. YOLOX-based blue laser weeding robot in corn field. Frontiers in Plant Science, 2022; 13.
[13] Keller M D, Norton B J, Farrar D J, Rutschman P, Marvit M, Makagon A. Optical tracking and laser-induced mortality of insects during flight. Scientific Reports, 2020; 10: 14795.
[14] Sun T, Liu B, Zheng R, Peng Z. Research on multi-target recognition and classification strategy based on Yolo V5 framework. The Proceedings of the 2021 Asia-Pacific International Symposium on Aerospace Technology (APISAT 2021). 2023; 2: 989–1002. doi: 10.1007/978-981-19-2635-8_73.
[15] Viswanatha V, Chandana R K, Ramachandra A C. Real time object detection system with Yolo and CNN models: A review. Journal of Xi'an University of Architecture & Technology, 2022; 14(7): 144–151.
[16] Wang Z, Jin L, Wang S, Xu H. Apple stem/calyx real-time recognition using YOLO-v5 algorithm for fruit automatic loading system. Postharvest Biology and Technology, 2022; 185: 111808.
[17] Wen H, Dai F, Yuan Y. A Study of YOLO Algorithm for Target Detection. 26th International Conference on Artificial Life and Robotics (ICAROB), 2021; 26: 622–625. doi: 10.5954/ICAROB.2021.OS13-9
[18] Yue X, Wang Q, He L, Li Y, Tang D. Research on tiny target detection technology of fabric defects based on improved YOLO. Applied Sciences, 2022; 12(13): 6823.
[19] Lv F, Liu B, Lu F. Attention guided low-light image enhancement with a large scale low-light simulation dataset. International Journal of Computer Vision, 2021; 129: 2175–2193.
[20] Hu W-C, Lin C-H. Field of view alignment with multiple RGB-D cameras. 2013 IEEE International Symposium on Consumer Electronics (ISCE), 2013: pp.169–170. doi: 10.1109/ISCE.2013.6570166.
[21] Curto E, Araujo H. 3D reconstruction of deformable objects from RGB-D cameras: An omnidirectional inward-facing multi-camera system. 16th International Joint Conference on Computer Vision, Imaging and Computer Graphics Theory and Applications (VISIGRAPP)/ 16th International Conference on Computer Vision Theory and Applications (VISAPP). 2021; 4: 544–551. doi: 10.5220/0010347305440551
[22] Liu W, Li F, Jing C, Wan Y, Su B, Helali M. Recognition and location of typical automotive parts based on the RGB-D camera. Complex & Intelligent Systems, 2021; 7: 1759–1765.
[23] Gritsenko I, Seidakhmet A, Abduraimov A, Gritsenko P, Bekbaganbetov A. delta robot forward kinematics method with one root. International Conference on Robotics and Automation Sciences (ICRAS), 2017; pp.39–42. doi: 10.1109/ICRAS.2017.8071913.
[24] Jiang H, Leng J, Niu Z. Structural design and efficient workspace optimization of a four-bar delta parallel picking robot. 2nd International Conference on Artificial Intelligence and Information Systems (ICAIIS), 2021; 10: 1–8. doi: 10.1145/3469213.3469223.
[25] Hovi A, Forsström P, Möttus M, Rautiainen M. Evaluation of accuracy and practical applicability of methods for measuring leaf reflectance and transmittance spectra. Remote Sensing, 2018; 10(1): 25.
[26] Zheng J, Hu M J, Guo Y P. Regulation of photosynthesis by light quality and its mechanism in plants. Chinese Journal of Applied Ecology, 2008; 19(7): 1619–1624.
[27] Berdnik V V, Mukhamedyarov R D. Radiative transfer in plant leaves. Optics and Spectroscopy, 2001; 90(4): 580–591.
[28] Bi S. Discuss wave-particle duality of light. 2nd International Conference on Photonics and Optical Engineering, 2017; 10256. doi: 10.1117/12.2260702.
[29] Sánchez H R. Seven derivations of the Beer-Lambert law. Spectroscopy Letters, 2021; 54(2): 133–139.
[30] Schansker G, Srivastava A, Govindjee, Strasser R J. Characterization of the 820-nm transmission signal paralleling the chlorophyll a fluorescence rise (OJIP) in pea leaves. Functional Plant Biology, 2003; 30(7): 785–796.
[31] Albrecht H, Fiorani F, Pieruschka R, Müller-Linow M, Jedmowski C, Schreiber L, et al. Quantitative estimation of leaf heat transfer coefficients by active thermography at varying boundary layer conditions. Frontiers in Plant Science, 2020; 10.
[32] Shi Y, Ke X, Yang X, Liu Y, Hou X. Plants response to light stress. Journal of Genetics and Genomics, 2022; 49(8): 735–747.
[33] Shafiq I, Hussain S, Raza M A, Iqbal N, Asghar M A, Raza A, et al. Crop photosynthetic response to light quality and light intensity. Journal of Integrative Agriculture, 2021; 20(1): 4–23.
[34] Chalker B E. Modelling light saturation curves for photosynthesis: An exponential function. Journal of theoretical biology, 1980; 84(2): 205–215.
[35] Allahverdiyeva Y, Aro E-M. Photosynthetic responses of plants to excess light: mechanisms and conditions for photoinhibition, excess energy dissipation and repair. Photosynthesis: Plastid Biology, Energy Conversion and Carbon Assimilation. Advances in Photosynthesis and Respiration, 2012; 34: 275–297. doi: 10.1007/978-94-007-1579-0_13.
[36] Zhang J, Xie S, Yan S, Xu W, Chen J. Light energy partitioning and photoprotection from excess light energy in shade-tolerant plant *Amorphophallus xiei* under steady-state and fluctuating high light. Acta Physiologiae Plantarum, 2021; 43(125).
[37] Brudvig G W, Tracewell C A, Lakshmi K V, Reifler M J, Stewart D H, Cua A, et al. Carotenoid and chlorophyll photooxidation in photosystem II. Photosynthesis Research, 2001; 69(1-3): 51.
[38] Osmond B, Badger M, Maxwell K, Björkman O, Leegood R. Too many photos: photorespiration, photoinhibition and photooxidation. Trends in Plant Science, 1997; 2(4): 119–121.
[39] Zhang S, Li C, Cao L, Moser M A J, Zhang W, Qian Z, et al. Modeling and *ex vivo* experimental validation of liver tissue carbonization with laser ablation. Computer Methods and Programs in Biomedicine, 2022; 217: 106697.